LETTERS

An excitable gene regulatory circuit induces transient cellular differentiation

Gürol M. Süel[1], Jordi Garcia-Ojalvo[2], Louisa M. Liberman[1] & Michael B. Elowitz[1]

Certain types of cellular differentiation are probabilistic and transient[1–3]. In such systems individual cells can switch to an alternative state and, after some time, switch back again. In *Bacillus subtilis,* competence is an example of such a transiently differentiated state associated with the capability for DNA uptake from the environment. Individual genes and proteins underlying differentiation into the competent state have been identified[4,5], but it has been unclear how these genes interact dynamically in individual cells to control both spontaneous entry into competence and return to vegetative growth. Here we show that this behaviour can be understood in terms of excitability in the underlying genetic circuit. Using quantitative fluorescence time-lapse microscopy, we directly observed the activities of multiple circuit components simultaneously in individual cells, and analysed the resulting data in terms of a mathematical model. We find that an excitable core module containing positive and negative feedback loops can explain both entry into, and exit from, the competent state. We further tested this model by analysing initiation in sister cells, and by re-engineering the gene circuit to specifically block exit. Excitable dynamics driven by noise naturally generate stochastic and transient responses[6], thereby providing an ideal mechanism for competence regulation.

Upon encountering nutrient limitation, a minority of *B. subtilis* cells become competent for DNA uptake while most commit irreversibly to sporulation (Fig. 1a). Extensive research has elucidated a detailed map of molecular interactions that comprise the *B. subtilis* competence control circuit (Supplementary Fig. S1)[4,5]. At the heart of this circuit is the ComK 'master' transcription factor (Fig. 1b). ComK activates expression of a suite of genes necessary for competence, including the *comG* operon (Fig. 1b)[7–10]. ComK also activates its own expression, and two recent studies have shown that this positive feedback loop is critical for the induction of competence[11,12]. Upon entry into stationary phase, *comK* is expressed at a basal level, but is also rapidly degraded by the MecA complex, a multiprotein assembly that includes the ClpP–ClpC proteases[13]. Independent studies have shown that the ComS peptide competitively inhibits ComK degradation by the MecA complex[13,14]. Expression of ComS thus favours induction of competence by allowing ComK levels to build up sufficiently to enable full ComK activation by positive autoregulation. Despite the important role of ComS in inducing competence, its expression is activated by stress and cell–cell signalling and is therefore high in all cells under stress, not just those destined to become competent[7]. Interestingly, overexpression of ComK was suggested to suppress expression of *comS*[7]. This implies the existence of an indirect negative feedback loop acting upon ComK, which might affect exit from competence (Fig. 1b). Therefore, we consider here interactions among the MecA complex, *comK* and *comS*, which we collectively refer to as the 'MeKS' module.

Differentiation into the competent state is difficult to study by traditional methods that average over large populations: the process affects a small minority of cells in a non-synchronous manner. Here we built strains in which activities of different pairs of promoters within the circuit could be monitored simultaneously in the same cell, revealing interactions between circuit components that could not be obtained by observing the same genes one at a time. Pairwise combinations of the promoters P_{comG}, P_{comK} and P_{comS} expressing *yfp* or *cfp* were inserted into standard sites within the *B. subtilis* chromosome, leaving the endogenous genes intact (see Supplementary Information). We analysed these strains using automated time-lapse fluorescence microscopy, and quantitative image analysis[15], under conditions where the overall frequency of competence events was $3.6 \pm 0.7\%$ (26 out of 725 cell division events generated competent cells).

The resulting data can be interpreted in terms of a mathematical model of the MeKS module. As described in Box 1, the MeKS model is a dynamical system that exhibits excitability: relatively small, threshold-crossing perturbations trigger large-amplitude excursions in phase space that eventually return the system to its initial state[6]. Correspondingly, in the cell, stochastic effects in gene expression have been shown to generate significant variability[16,17]. Such biochemical 'noise' can initiate a sequence of intracellular events—changes in gene expression and protein degradation—that cause cells to transiently differentiate into the competent state and subsequently return to vegetative growth. Noise-driven excitable systems naturally exhibit the two key characteristics of competence: probabilistic and transient activation.

To explore these properties further, we first simultaneously measured P_{comG} and P_{comK} promoter activities in single competent cells. P_{comG} and P_{comK} are both regulated by ComK, but P_{comK} also has many other important transcriptional inputs (Supplementary Fig. S1). This experiment evaluates the significance of these other transcriptional inputs into P_{comK} during competence. Figure 2a shows frames from recorded film footage of a *B. subtilis* microcolony under nutrient limitation conditions, in which most cells eventually sporulate (see also Supplementary Movie 1). In this example, a single cell within the microcolony becomes competent and consequently its cell division is blocked, as previously reported[18]. As P_{comG} and P_{comK} activities decline during exit from competence, the elongated cell undergoes multiple septation events and returns to the vegetative state. Quantitative time traces of the fluorescence levels show strong correlation between P_{comG} and P_{comK} in this film footage (Fig. 2b). This behaviour is representative of all measured events in this strain ($n = 37$) (Fig. 2c). The high degree of correlation between P_{comG} and P_{comK} suggests that other transcriptional inputs to the ComK promoter do not significantly affect ComK expression during competence.

In the MeKS model, ComK indirectly represses ComS, generating an anti-correlation between P_{comG} and P_{comS} activities. The regulation

[1]Division of Biology and Department of Applied Physics, California Institute of Technology, Pasadena, California 91125, USA. [2]Departament de Física i Enginyeria Nuclear, Universitat Politècnica de Catalunya, Colom 11, E-08222 Terrassa, Spain.

of *comS* is, however, known to be complex, having several transcriptional inputs (Supplementary Fig. S1)[19–21]. To test the prediction of the MeKS model we constructed a strain containing copies of the P_{comG} and P_{comS} promoters expressing *cfp* and *yfp*, respectively. As shown in Fig. 3a and Supplementary Movie 2, all cells express P_{comS} to varying degrees. In cells that become competent, P_{comG} activity increases as P_{comS} activity decreases. Later, as P_{comG} activity shuts off and septation begins, P_{comS} activity increases again. This striking negative correlation between P_{comG} and P_{comS} activities is present during both entry and exit from competence, although it is more closely synchronized during entry (Fig. 3b). This behaviour is representative of data obtained from all competent cells of the same strain ($n = 31$) (Fig. 3c), and is consistent with negative regulation of *comS* by ComK. Furthermore, the negative correlation is specific to competence, as is evident from the behaviour of the non-competent sister cell in Fig. 3b.

A fundamental question is whether initiation of competence is stochastic or affected by memory of previous events. Escape from competence returns promoter activities to pre-competence levels, suggesting the possibility of successive episodes of competence. Indeed, as shown in Fig. 3d, two consecutive competence events can be observed in a single cell lineage, showing that cells retain the potential to re-initiate competence. In fact, re-initiation occurred with a frequency of 6.0 ± 2.0% ($n = 9$ events out of 151), not significantly different from the overall competence frequency (3.6 ± 0.7%). Repeated competence events are neither favoured nor suppressed. This evidence for stochastic initiation of competence is further supported by analysis of competence events in sister cell pairs (Supplementary Information). Cells were not significantly more or less likely to become competent if their sister became competent (conditional frequency = 4.1 ± 0.9%, $n = 19$ events out of 463). When two sisters do become competent together, the amount of time one spends in competence is uncorrelated with that of its sister cell (Kolmogorov–Smirnov test; $n = 36$). These results are consistent with a stochastic and memory-less model for competence initiation and duration.

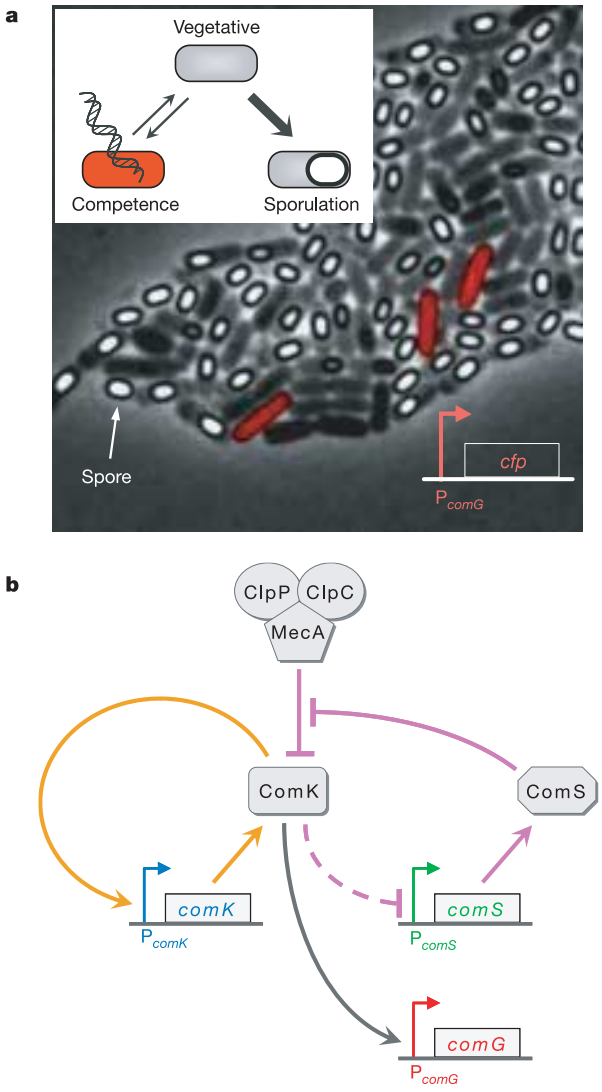

Figure 1 | Stress response in *B. subtilis* and the core competence circuit. **a**, Snapshot of a *B. subtilis* microcolony in nutrient-limited conditions. *cfp* expression from P_{comG} is shown in red. Inset: a flow chart illustrating developmental paths connecting the vegetative, spore forming and competent states. **b**, Map of interactions within the core competence circuit (MeKS). The transcriptional autoregulatory positive feedback loop of ComK and the ComS-mediated indirect negative feedback loop are depicted in orange and purple, respectively. ComS competes with ComK for degradation by the MecA–ClpP–ClpC complex, effectively interfering with degradation of ComK (curved purple inhibitory arrow). The dashed purple line from ComK to P_{comS} denotes indirect repression. The activities of the promoters labelled in red, blue and green were measured in this study. These colours are used to represent the corresponding promoters throughout the figures.

Box 1 | The dynamical model of competence induction

To understand how the MeKS network structure determines the dynamics of competence, we built a mathematical model constrained by experimental observations (see Supplementary Information). This model can be reduced to a system of two stochastic ordinary differential equations incorporating both the direct positive and the ComS-mediated negative feedback loops of ComK. In dimensionless form:

$$\frac{dK}{dt} = a_k + \frac{b_k K^n}{k_0^n + K^n} - \frac{K}{1+K+S} \quad (1)$$

$$\frac{dS}{dt} = \frac{b_s}{1+(K/k_1)^p} - \frac{S}{1+K+S} + \xi(t) \quad (2)$$

Here, K and S represent the concentration levels of ComK and ComS protein, respectively. a_k and b_k represent minimal and fully activated rates of ComK production, respectively. k_0 is the concentration of ComK required for 50% activation. The cooperativities of ComK auto-activation and ComS repression are parameterized by the Hill coefficients n and p, respectively. Expression of ComS has maximum rate b_s and is half-maximal when $K = k_1$. Enzymatic MecA-mediated degradation affects both ComK and ComS; the form of the corresponding nonlinear degradation terms expresses a competitive mechanism, which is the only source of coupling from ComS to ComK. Random fluctuations in ComS expression are represented by a noise term $\xi(t)$ (see Supplementary Information for a more detailed analysis).

The dynamical behaviour of equations (1) and (2) without noise can be analysed graphically by plotting their nullclines and vector field in the ComK–ComS phase space (Fig. 4a) for appropriate parameters (given in the Supplementary Information). This analysis reveals three fixed points: a stable node at low ComK (the vegetative state) and two unstable fixed points. Of these, the one at intermediate ComK is an unstable saddle and the one at high ComK (the competent state) is an unstable spiral. No limit-cycle behaviour coexists with the stable vegetative state in this parameter region (see Supplementary Information). Under these conditions, the system is capable of excitable behaviour: relatively small perturbations from the vegetative state may cause long excursions through phase space around the unstable spiral at high ComK (that is, through the competence region), as determined by the vector field. The vegetative state can be perturbed by noise in the expression of either ComK or ComS, leading to these transient differentiation events. Samples of such trajectories, generated by numerical integration of the model, are superimposed as pink lines in Fig. 4a and plotted against time in Fig. 4b.

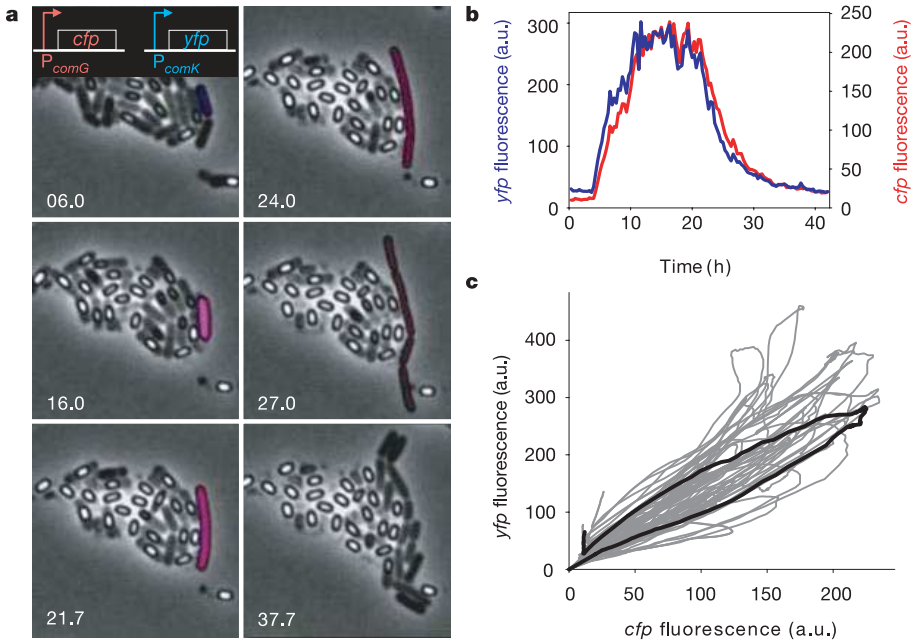

Figure 2 | Activities of P_{comK} and P_{comG} promoters are highly correlated during competence. **a**, Frames from film footage of a typical competence event. *yfp* expressed from P_{comK} and *cfp* expressed from P_{comG} are coloured blue and red, respectively (see also Supplementary Movie 1). Overlapping dynamics of P_{comK} and P_{comG} result in the purple (red plus blue) colour of the competent cell. Time (in hours) is indicated for each frame. **b**, Quantitative time series of P_{comK}–*yfp* (blue line) and P_{comG}–*cfp* (red line) obtained through semi-automated data processing of the competence event shown in **a**. P_{comK} and P_{comG} activities exhibit nearly identical dynamics. a.u., arbitrary units. **c**, Plot of P_{comK}–*yfp* versus P_{comG}–*cfp* obtained from all ($n = 37$) competence events in this strain. The traces are smoothed for visual clarification. Note the positive correlation between P_{comK}–*yfp* and P_{comG}–*cfp*. Highlighted in black is the competence time trace depicted in **b**.

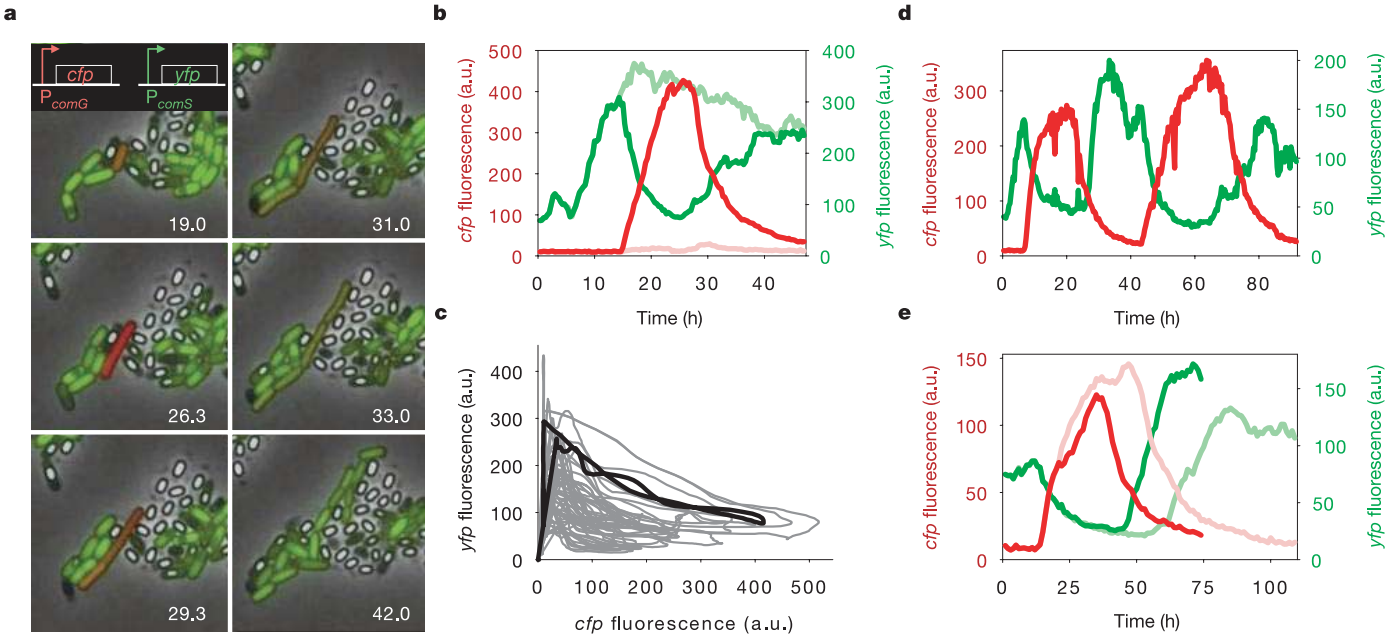

Figure 3 | Promoter activities of P_{comS} and P_{comG} are anti-correlated during competence. **a**, Frames from film footage of a typical competence event with P_{comS}–*yfp* and P_{comG}–*cfp* expression shown in green and red, respectively (see inset) (see also Supplementary Movie 2). Time (in hours) is indicated for each frame. **b**, Quantitative time series of P_{comS}–*yfp* (green line) and P_{comG}–*cfp* (red lines) for the competence event shown in **a**. Depicted in faint green and faint red are P_{comS} and P_{comG} activities obtained from the non-competent sister cell. Note that the negative correlation between P_{comS} and P_{comG} expression dynamics is only observed in the competent cell. **c**, Plot of P_{comS}–*yfp* versus P_{comG}–*cfp* obtained from all ($n = 31$) competence events in this strain. The traces are smoothed for visual clarification. Note the negative correlation between P_{comS}–*yfp* and P_{comG}–*cfp*. Highlighted in black is the competence time trace depicted in **b**. **d**, Quantitative time traces of consecutive competence events within a single cell lineage. The colour scheme is identical to that described for **b**. **e**, Quantitative time traces of P_{comS}–*yfp* and P_{comG}–*cfp* measured in sister cells that both undergo competence. The colour scheme is identical to that described for **b**. Note the different durations of competence in sister cells (see Supplementary Fig. S7).

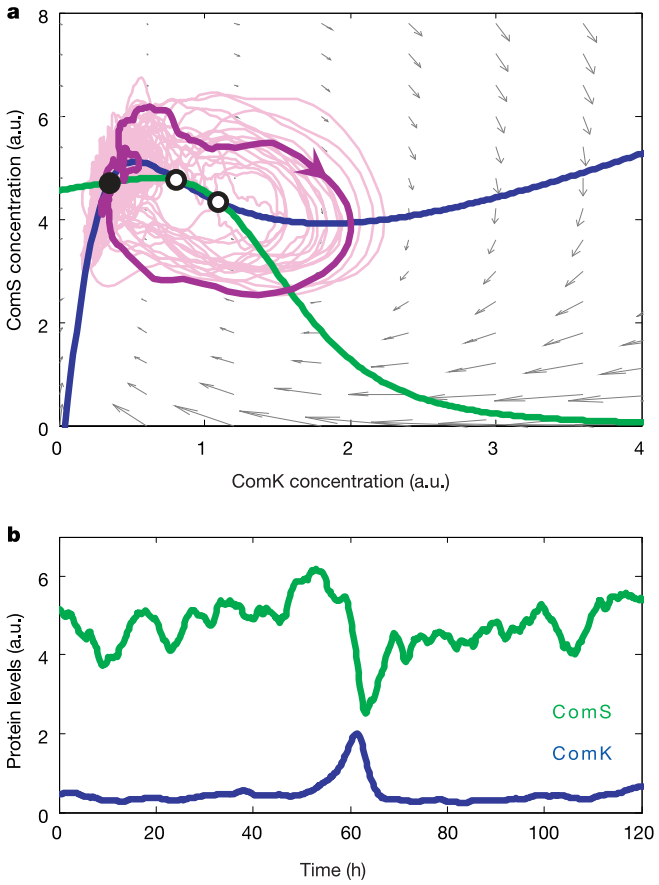

Figure 4 | Modelling of the core competence network reveals an excitable system. a, Phase plane diagram formed by the system of equations shown in Box 1. Nullclines for equations (1) and (2) are shown in blue and green, respectively. Grey arrows represent the vector field of the dynamical system. The stable steady-state corresponding to vegetative growth is indicated with a black filled circle. The saddle and the unstable competent fixed points are indicated with open circles. A set of excursion trajectories is shown in pink, with a single representative trajectory of the system highlighted in purple. Initiation of excursions in phase space is triggered by noise (Box 1), and trajectories are determined by the phase space vector field. **b**, Simulations of ComS (green) and ComK (blue) activities as a function of time. Note the negative correlation between the ComS and ComK levels during competence, consistent with experimental observations.

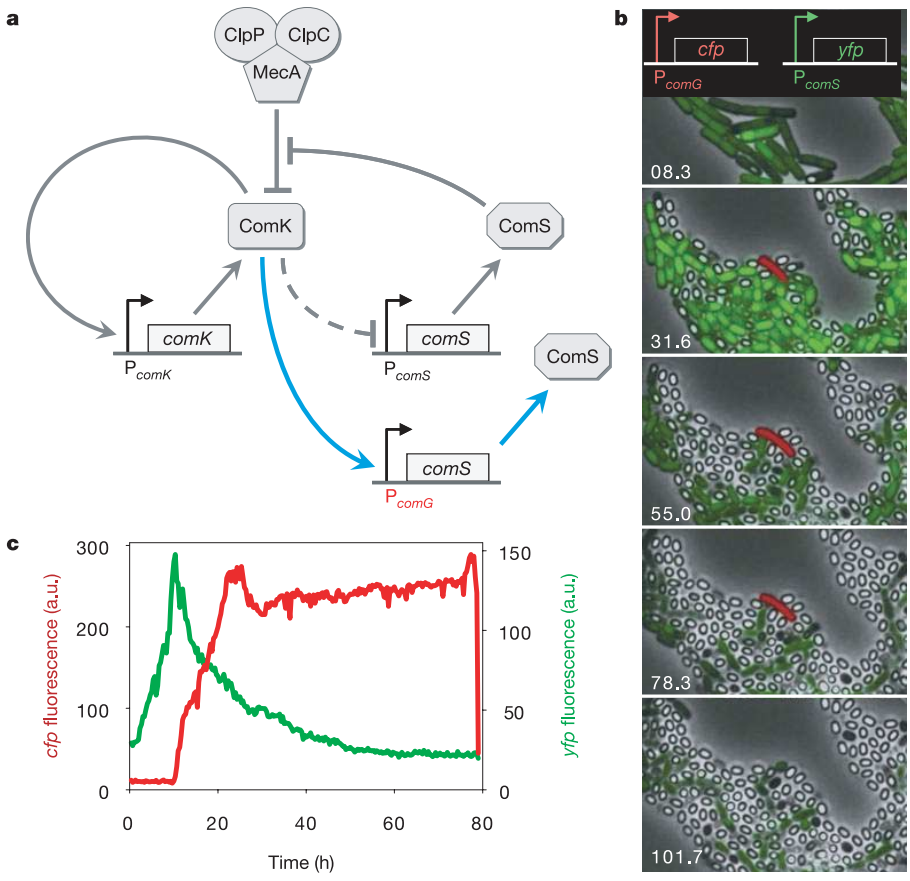

Figure 5 | Competence lock through feedback bypass. a, Network schematic depicting in blue the extra link introduced to bypass the native ComS-mediated negative feedback loop (FeBy strain). Note that the native network is left intact (see Fig. 1a). **b**, Frames from film footage of a typical competence event in the FeBy strain, with P_{comS} and P_{comG} activities depicted in green and red, respectively (see also Supplementary Movie 3). **c**, Quantitative time series of P_{comS}–*yfp* (green line) and P_{comG}–*cfp* (red line) for the event shown in **b**. The FeBy cell enters competence, but cannot exit from competence and eventually lyses (note the sudden drop after nearly 80 h).

To understand how the network structure supports the dynamics of competence, we built a differential equation model of the MeKS module that incorporates noise. In this model, two feedback loops regulate ComK: the positive loop is based on direct transcriptional auto-activation; the negative loop is indirect and involves ComS-modulated degradation of ComK (Fig. 1a, Box 1 and Supplementary Information). This model contains a regime in which noise in the production of either ComK or ComS can trigger large excursions in phase space that resemble experimental observations (Fig. 4). Thus, this model of excitability accounts in a natural way for the dynamics of competence observed in experiments.

How does the circuit generate transient competence events? This behaviour is caused by the combination of a fast positive and slow negative feedback. Positive feedback motifs are well known generators of bistability in cell biology[22,23]. Combinations of positive and negative feedbacks are crucial elements of dynamic processes in biology such as the cell cycle[24]. In the present system, noise can induce escape from the otherwise stable vegetative state and turn the system 'on' via the ComK positive feedback, as suggested previously by other groups[11,12]. On a slower timescale, this initiates the ComS-mediated negative feedback. Reduction in ComS levels eventually shuts the system back 'off' through an increase in ComK degradation, returning the cell to its vegetative state. In this way, ComS has a dual role in the system: on the one hand it is necessary to initiate competence, by blocking degradation of ComK and allowing positive autoregulation to take effect; on the other hand, repression of ComS is necessary for exit from competence, because reduction in ComS levels favours ComK degradation by MecA.

The excitable model of competence induction makes a strong prediction: interfering with the ComS-mediated negative feedback loop should stabilize the competent state without changing the frequency with which cells become competent (Supplementary Fig. S6). To test this prediction, we constructed a feedback bypass (FeBy) strain of *B. subtilis* containing a single chromosomal copy of P_{comG} driving the expression of *comS* (Fig. 5a). This modification leaves the native competence network intact: the added *comS* gene is expressed only in competent cells. By expressing additional ComS in this way, the natural negative feedback is rendered ineffective.

We performed time-lapse microscopy on the FeBy strain (Fig. 5b and Supplementary Movie 3). The resulting movies show that FeBy cells become competent at normal frequencies ($4.2 \pm 0.8\%$; $n = 32$ out of 754), but most of these competent cells fail to return to vegetative growth. In a wild-type culture, 61% of cells successfully exit competence ($n = 136$), compared to only 12% of FeBy cells ($n = 55$). P_{comG} expression levels in competent FeBy cells do not significantly exceed those in wild-type cells, suggesting that the defect in exit is not simply due to overexpression of ComK. As in wild-type cells, a negative correlation between P_{comG} and P_{comS} is observed in FeBy cells (Fig. 5c). Thus, the FeBy cells behave similarly to wild-type cells during entry into competence, and differ specifically in their reduced ability to exit.

Even in well-characterized cellular networks, it is generally difficult to connect circuit structure to circuit dynamics[25]. Within the complex *B. subtilis* competence circuitry however, the relatively simple MeKS module can explain the transient and probabilistic features of competence dynamics. This suggests that during competence not all of the known interactions within the larger competence circuit are important all of the time.

In the FeBy strain, a single rewiring step transformed a transient differentiation process into a terminal one. This reflects a degree of plasticity in the excitable circuit module. Notably, the architecture of this circuit is similar to the circadian clock and cell cycle oscillators, which also contain combined positive–negative feedback loops[24,26,27]. Excitability is found in biological systems that process information such as neurons, where the frequency of events, but not their shape or amplitude, needs to be tuned[28]. Our results show that excitability also operates in an intracellular genetic network controlling transient differentiation—an event on a very different timescale that uses completely different molecular components. Evidently, analogous functional roles for excitable dynamics exist in microbial and neuronal systems. We anticipate that this circuit design may therefore represent a general solution to a range of biological design problems.

METHODS

For detailed information on all methods, see Supplementary Information

Strain construction. Promoter–*yfp*/*cfp* fusions were generated using fusion polymerase chain reaction techniques and cloned into *B. subtilis* integration vectors pDL30 (gift from J. Dworkin), pPyr-Cm and pSac-Cm (constructed by R. Middleton). The strain background was *B. subtilis* strain PY79.

Preparation of cells for microscopy. Cells were grown at 37 °C in Luria broth to an optical density of 1.8 and re-suspended in 0.5 volume of resuspension medium (RM) supplemented with 0.02% glucose. After 1.5 h incubation at 37 °C, cells were applied onto a 1.5% agarose pad made with RM and placed into a coverslip-bottom Willco dish for imaging.

Time-lapse microscopy. Growth of microcolonies was observed with fluorescence time-lapse microscopy at 37 °C using an Olympus IX-81 inverted microscope with a motorized stage (ASI). Image sets were acquired every 20 min with a Hamamatsu ORCA-ER camera. Custom Visual Basic software was used to automate image acquisition and microscope control.

Data analysis. Time-lapse microscopy data were analysed with custom software written in Matlab.

Model analysis. Mathematical models were simulated using custom-made software and further analysed using the analytic continuation software packages AUTO and DDE-BIFTOOL.

Received 15 September 2005; accepted 18 January 2006.

1. Dupin, E., Real, C., Glavieux-Pardanaud, C., Vaigot, P. & Le Douarin, N. M. Reversal of developmental restrictions in neural crest lineages: transition from Schwann cells to glial-melanocytic precursors *in vitro*. *Proc. Natl Acad. Sci. USA* **100,** 5229–5233 (2003).
2. Lee, E. J., Russell, T., Hurley, L. & Jameson, J. L. Pituitary transcription factor-1 induces transient differentiation of adult hepatic stem cells into prolactin-producing cells *in vivo*. *Mol. Endocrinol.* **19,** 964–971 (2005).
3. Meeks, J. C., Campbell, E. L., Summers, M. L. & Wong, F. C. Cellular differentiation in the cyanobacterium *Nostoc punctiforme*. *Arch. Microbiol.* **178,** 395–403 (2002).
4. Grossman, A. D. Genetic networks controlling the initiation of sporulation and the development of genetic competence in *Bacillus subtilis*. *Annu. Rev. Genet.* **29,** 477–508 (1995).
5. Hamoen, L. W., Venema, G. & Kuipers, O. P. Controlling competence in *Bacillus subtilis*: shared use of regulators. *Microbiology* **149,** 9–17 (2003).
6. Lindner, B., Garcia-Ojalvo, J., Neiman, A. & Schimansky-Geier, L. Effects of noise in excitable systems. *Phys. Rep.* **392,** 321–424 (2004).
7. Hahn, J., Kong, L. & Dubnau, D. The regulation of competence transcription factor synthesis constitutes a critical control point in the regulation of competence in *Bacillus subtilis*. *J. Bacteriol.* **176,** 5753–5761 (1994).
8. Hahn, J., Luttinger, A. & Dubnau, D. Regulatory inputs for the synthesis of ComK, the competence transcription factor of *Bacillus subtilis*. *Mol. Microbiol.* **21,** 763–775 (1996).
9. van Sinderen, D. *et al. comK* encodes the competence transcription factor, the key regulatory protein for competence development in *Bacillus subtilis*. *Mol. Microbiol.* **15,** 455–462 (1995).
10. van Sinderen, D. & Venema, G. *comK* acts as an autoregulatory control switch in the signal transduction route to competence in *Bacillus subtilis*. *J. Bacteriol.* **176,** 5762–5770 (1994).
11. Maamar, H. & Dubnau, D. Bistability in the *Bacillus subtilis* K-state (competence) system requires a positive feedback loop. *Mol. Microbiol.* **56,** 615–624 (2005).
12. Smits, W. K. *et al.* Stripping *Bacillus*: ComK auto-stimulation is responsible for the bistable response in competence development. *Mol. Microbiol.* **56,** 604–614 (2005).
13. Turgay, K., Hahn, J., Burghoorn, J. & Dubnau, D. Competence in *Bacillus subtilis* is controlled by regulated proteolysis of a transcription factor. *EMBO J.* **17,** 6730–6738 (1998).
14. Ogura, M., Liu, L., Lacelle, M., Nakano, M. M. & Zuber, P. Mutational analysis of ComS: evidence for the interaction of ComS and MecA in the regulation of competence development in *Bacillus subtilis*. *Mol. Microbiol.* **32,** 799–812 (1999).
15. Rosenfeld, N., Young, J. W., Alon, U., Swain, P. S. & Elowitz, M. B. Gene regulation at the single-cell level. *Science* **307,** 1962–1965 (2005).
16. Ozbudak, E. M., Thattai, M., Kurtser, I., Grossman, A. D. & van Oudenaarden, A. Regulation of noise in the expression of a single gene. *Nature Genet.* **31,** 69–73 (2002).
17. Elowitz, M. B., Levine, A. J., Siggia, E. D. & Swain, P. S. Stochastic gene expression in a single cell. *Science* **297,** 1183–1186 (2002).

18. Haijema, B. J., Hahn, J., Haynes, J. & Dubnau, D. A. ComGA-dependent checkpoint limits growth during the escape from competence. *Mol. Microbiol.* **40,** 52–64 (2001).
19. Serror, P. & Sonenshein, A. L. CodY is required for nutritional repression of *Bacillus subtilis* genetic competence. *J. Bacteriol.* **178,** 5910–5915 (1996).
20. Nakano, M. M. & Zuber, P. The primary role of *comA* in establishment of the competent state in *Bacillus subtilis* is to activate expression of *srfA*. *J. Bacteriol.* **173,** 7269–7274 (1991).
21. Hahn, J. & Dubnau, D. Growth stage signal transduction and the requirements for *srfA* induction in development of competence. *J. Bacteriol.* **173,** 7275–7282 (1991).
22. Isaacs, F. J., Hasty, J., Cantor, C. R. & Collins, J. J. Prediction and measurement of an autoregulatory genetic module. *Proc. Natl Acad. Sci. USA* **100,** 7714–7719 (2003).
23. Xiong, W. & Ferrell, J. E. Jr. A positive-feedback-based bistable 'memory module' that governs a cell fate decision. *Nature* **426,** 460–465 (2003).
24. Pomerening, J. R., Kim, S. Y. & Ferrell, J. E. Jr. Systems-level dissection of the cell-cycle oscillator: bypassing positive feedback produces damped oscillations. *Cell* **122,** 565–578 (2005).
25. Lahav, G. *et al.* Dynamics of the p53-Mdm2 feedback loop in individual cells. *Nature Genet.* **36,** 147–150 (2004).
26. Hardin, P. E. The circadian timekeeping system of *Drosophila*. *Curr. Biol.* **15,** R714–R722 (2005).
27. Vilar, J. M., Kueh, H. Y., Barkai, N. & Leibler, S. Mechanisms of noise-resistance in genetic oscillators. *Proc. Natl Acad. Sci. USA* **99,** 5988–5992 (2002).
28. Keener, J. & Sneyd, J. *Mathematical Physiology* (Springer, New York, 1998).

Supplementary Information is linked to the online version of the paper at www.nature.com/nature.

Acknowledgements We thank U. Alon, D. Dubnau, J. Dworkin, A. Eldar, J. Ferrell, R. Kishony, B. Lazazzera, R. Losick, A. Raj, B. Shraiman, D. Sprinzak, M. Surette and members of the laboratory for comments. G.M.S. is supported by the Caltech Center for Biological Circuit Design. J.G.-O. acknowledges financial support from the Generalitat de Catalunya and the Ministerio de Educacion y Ciencia (Spain). M.B.E. acknowledges support from the Searle Scholars Program and the Burroughs Wellcome Fund CASI program.

Author Information Reprints and permissions information is available at npg.nature.com/reprintsandpermissions. The authors declare no competing financial interests. Correspondence and requests for materials should be addressed to M.B.E. (melowitz@caltech.edu).

SUPPLEMENTARY INFORMATION

AN EXCITABLE GENE REGULATORY CIRCUIT INDUCES TRANSIENT CELLULAR DIFFERENTIATION

Gürol M. Süel,[1] Jordi Garcia-Ojalvo,[2] Louisa L. Liberman,[1] and Michael B. Elowitz[1]

[1]*Division of Biology and Department of Applied Physics, California Institute of Technology, Pasadena, CA 91125*

[2]*Departament de Física i Enginyeria Nuclear, Universitat Politècnica de Catalunya, Colom 11, 08222 Terrassa, Spain*

Contents

S1. MATERIALS AND METHODS

S1.A. Cloning and strain construction

Polymerase Chain Reaction (PCR) was utilized to amplify native P_{comK}, P_{comG} and P_{comS} promoters as well as *comS* from the wild type *B. subtilis* PY79 strain (kind gift from Jonathan Dworkin) using Pfx DNA polymerase (Invitrogen). For each of the promoters, we amplified the entire sequence between the ribosome binding site and the preceeding structural gene. These products were then used to generate promoter-*yfp/cfp* (*yfp* and *cfp* were obtained from pDH5 plasmid and University of Washington Yeast Resource Center, respectively) and P_{comG}-*comS* fusions. All of these constructs were obtained using standard fusion PCR techniques with Pfx and cloned into *B. subtilis* integration vectors. We used *BamH1* and *EcoR1* sites within the pDL30 (kind gift from Jonathan Dworkin), pPyr-Cm, pSac-Cm (constructed by R. Middleton and obtained from the *B. subtilis* Stock Center) integration vectors for cloning. Standard *B. subtilis* transformation protocols were followed to transform *B. subtilis* strain PY79 with these plasmids. Integration of constructs into the chromosome were verified by PCR and sequencing. We incorporated several terminator sequences around the constructs to prevent read through transcription from chromosomal promoters near the integration sites. Furthermore, we observed no dependence of expression dynamics on integration site or orientation of the constructs with respect to the chromosome.

S1.B. Preparation of cells for microscopy

Cells were grown at 37°C in Luria Broth (LB) to an O.D. of 1.8 and resuspended in 0.5 volume of resuspension medium (RM) [S1] supplemented with 0.02% glucose. After 1.5 hour incubation at 37°C, cells were diluted 10-fold in RM and applied at appropriate densities (5-10 cells per field of view) onto a 1.5% low melting agarose pad made with RM and placed into a coverslip-bottom Willco dish. Willco dishes were sealed with parafilm to reduce evaporation from the agarose pads during the course of movie making. This protocol is optimized for time-lapse microscopy. RM reduces the growth rate of microcolonies on agarose and leads to sporulation. As a result, overgrowth of cells in the field of view is prevented, allowing the tracking of individual cell lineages for longer periods of time.

S1.C. Time-lapse microscopy

Growth of microcolonies was observed with fluorescence time-lapse microscopy at 37°C (temperature controlled chamber) using an Olympus IX-81 inverted microscope with a motorized stage (ASI). A Lambda-LS light source (Sutter Instruments) was used to excite fluorescence. Images were obtained with a Hamamatsu ORCA-ER camera. Custom written Visual Basic software was used to control the microscope and related equipment during the movie acquisition. Images were acquired every 20 minutes. Median cell cycle division times (excluding competence events) under these conditions are ∼200 minutes. We tested the effect of light exposure on cells and determined

that unfiltered exposure to the excitation light source lead to phototoxicity that resulted in the lysis of cells. We therefore used a combination of ultraviolet/infrared and neutral density filters to prevent phototoxicity. Even with these filters, acquisition rates faster than seven minutes per frame also resulted in phototoxicity-induced lysis. A typical dose response to light was determined (data not shown) by varying acquisition rates and counting lysis events. Frame rate (20 minutes) was chosen to minimize or eliminate such effects.

S1.D. Data analysis

Time-lapse microscopy movies were analyzed with the Matlab based custom made "schnitzcell" software package and other custom software [S2].

S1.E. Analysis in different growth conditions

Competence has previously been characterized in a specific medium [S3]. To determine the generality of our results we grew the P_{comG}-*cfp* / P_{comS}-*yfp* reporter strain in both RM media and traditional competence media (CM) [S3]. Cells grown in RM and CM were analyzed using fluorescence microscopy as described above. Microscopy images were quantified using Matlab-based custom written software, also described above. The resulting data are shown in Fig. S10 below. These data show that ComS is similarly repressed in both media.

S2. ANALYSIS OF THE DYNAMICAL MODEL

S2.A. Basic model of the competence module

The gene regulatory network underlying the development of competence in *B. subtilis* is shown in Fig. S1. On the basis of the assumptions made in the main text, we have concentrated on the simple module shown in Fig. 1 (main text). As discussed below, we have analyzed several variant models of this module and show that qualitatively similar results are obtained for all.

The interaction map within the core competent module (Fig. 1, main text) contains the following ingredients:

- ComK activates itself via a transcriptional autoregulatory positive feedback loop.
- ComK inhibits ComS expression via indirect transcriptional repression.
- MecA inhibits ComK via enzymatic degradation.
- The latter reaction is inhibited by ComS via competitive binding.

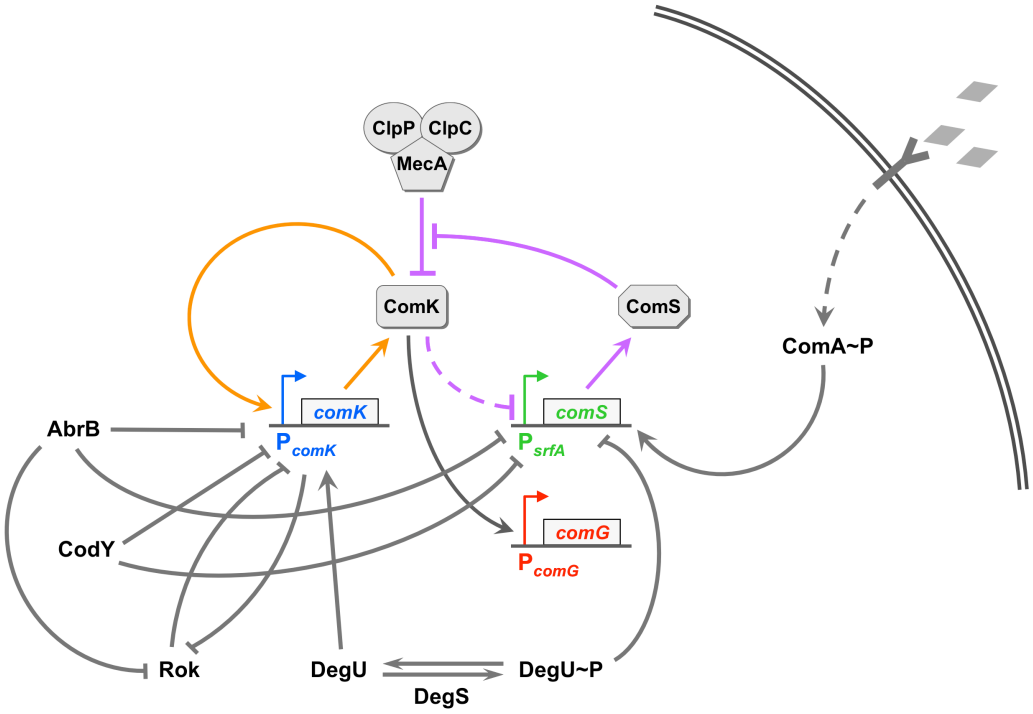

FIG. S1: Comprehensive map of molecular interactions within the *B. subtilis* competence network. Shown are selected genes and proteins within one link of the MeKS module. Transcriptional inputs to PcomK influence the fraction of competent cells in the population. AbrB is a global regulator that affects both sporulation and competence [S4]. CodY activity depends on intracellular GTP levels [S5]. Additionally, DegU/S is a two component system that also influences other stress responses such as swarming. The simplified MeKS model neglects these inputs because they do not appear to strongly influence the behavior of system once competence is initiated (see Fig. 2 in the main text). However, more detailed studies will be necessary to understand their role in the complete system.

ComK inhibits ComS expression by an effective Hill repression function [S2]. The enzymatic degradation reactions are assumed to be of the standard Michaelis-Menten form:

$$\begin{aligned} \text{MecA} + \text{ComK} &\overset{\gamma_{\pm a}}{\rightleftharpoons} \text{MecA-ComK} \overset{\gamma_1}{\rightarrow} \text{MecA} \\ \text{MecA} + \text{ComS} &\overset{\gamma_{\pm b}}{\rightleftharpoons} \text{MecA-ComS} \overset{\gamma_2}{\rightarrow} \text{MecA} \end{aligned}$$

Denoting by K and S the protein concentrations of ComK and ComS, respectively, and by M_f, M_K and M_S the concentrations of free MecA and of the complexes MecA-ComK and MecA-ComS, respectively, the dynamics of the network shown in Fig. 1 can be described by the following rate

equations:

$$\frac{dK}{dt} = \alpha_k + \frac{\beta_k K^n}{k_k^n + K^n} - \gamma_a M_f K + \gamma_{-a} M_K \tag{S1}$$

$$\frac{dS}{dt} = \frac{\beta_s}{1 + (K/k_s)^p} - \gamma_b M_f S + \gamma_{-b} M_S \tag{S2}$$

$$\frac{dM_K}{dt} = -(\gamma_{-a} + \gamma_1) M_K + \gamma_a M_f K \tag{S3}$$

$$\frac{dM_S}{dt} = -(\gamma_{-b} + \gamma_2) M_K + \gamma_b M_f K \tag{S4}$$

The meaning of the parameters are given in Table S1. In particular, the expression rate of ComS, β_s, can be expected to increase with nutrient limitation, since ComS expression is activated by starvation and cell crowding via the upstream protein ComA (see Fig. S1) [S6]. A differential equation for M_f is not necessary because we assume that the total amount of MecA is conserved:

$$M_f + M_K + M_S = M_{\text{total}} = \text{constant} \tag{S5}$$

Parameter	**Description**	**Value**
α_k	Basal expression rate of ComK	0.0028 nM/s
β_k	Saturating expression rate of ComK positive feedback	0.049 nM/s
β_s	Unrepressed expression rate of ComS	0.057 nM/s
k_k	ComK concentration for half-maximal ComK activation	100 nM
k_s	ComK concentration for half-maximal ComS repression	110 nM
δ_k	Unrepressed degradation rate of ComK	0.0014 s^{-1}
δ_s	Unrepressed degradation rate of ComS	0.0014 s^{-1}
Γ_k	ComK concentration for half-maximal degradation	500 nM
Γ_s	ComS concentration for half-maximal degradation	50 nM
n	Hill coefficient of ComK positive feedback	2
p	Hill coefficient of ComS repression by ComK	5

TABLE S1: Parameters of the dynamical model. The actual values of the parameters are obtained from the dimensionless parameters given in Table S2.

Assuming that γ_1^{-1} and γ_2^{-1} are much smaller than any other time scale in the system, we can adiabatically eliminate M_K and M_S. Therefore, taking the derivatives in Eqs. (S3)-(S4) equal to zero, and using relation (S5) leads to the reduced model:

$$\frac{dK}{dt} = \alpha_k + \frac{\beta_k K^n}{k_k^n + K^n} - \frac{\delta_k K}{1 + \frac{K}{\Gamma_k} + \frac{S}{\Gamma_s}} \tag{S6}$$

$$\frac{dS}{dt} = \frac{\beta_s}{1 + (K/k_s)^p} - \frac{\delta_s S}{1 + \frac{K}{\Gamma_k} + \frac{S}{\Gamma_s}} \tag{S7}$$

where

$$\Gamma_k = \frac{\gamma_{-a} + \gamma_1}{\gamma_a}, \qquad \Gamma_s = \frac{\gamma_{-b} + \gamma_2}{\gamma_b} \tag{S8}$$

and

$$\delta_k = \frac{\gamma_1 M_{\text{total}}}{\Gamma_k}, \qquad \delta_s = \frac{\gamma_2 M_{\text{total}}}{\Gamma_s} \tag{S9}$$

We have further assumed, without loss of generality, that the degradation rates δ_k and δ_s are equal. In that way, rescaling time with these rates and the concentrations of ComK and ComS with Γ_k and Γ_s, respectively, we obtain the dimensionless model:

$$\frac{dK}{dt} = a_k + \frac{b_k K^n}{k_0^n + K^n} - \frac{K}{1 + K + S} \tag{S10}$$

$$\frac{dS}{dt} = \frac{b_s}{1 + (K/k_1)^p} - \frac{S}{1 + K + S}\,, \tag{S11}$$

where now t, K and S are now dimensionless variables, and the dimensionless parameters of the model are defined as shown in Table S2. Reduction of the model to a set of two coupled differential equations allows a phase-plane analysis of the system dynamics, as described in what follows.

S2.B. Phase diagram

We now examine the dynamical behavior of model (S10)-(S11)[1]. The values chosen for the dimensionless parameters of the model are given in Table S2. These quantities translate into the real biochemical values listed in Table S1, determined by choosing the time unit $\delta_k^{-1} = \delta_s^{-1}$ to fit the experimentally observed excursion times (around 20 hours), and from educated guesses of the concentrations Γ_k and Γ_s.

Figure S2 shows the phase diagram of the model in the b_k-b_s plane. The diagram plots the number of fixed points in color coding, with red corresponding to three fixed points and blue to only one. In the blue area below the red region, the only fixed point is the vegetative state (low ComK), whereas in the area above, it is the competent state (high ComK). For the parameters chosen, the competent state undergoes a supercritical Hopf bifurcation (H) whose location, as computed with the continuation software AUTO [S8], is plotted in purple in the phase diagram. The green lines represent saddle-node (SN) bifurcations.

Parameter	**Definition**	**Value**
a_k	$\alpha_k/(\delta_k\Gamma_k)$	0.004
b_k	$\beta_k/(\delta_k\Gamma_k)$	0.07
b_s	$\beta_s/(\delta_s\Gamma_s)$	0.82
k_0	k_k/Γ_k	0.2
k_1	k_s/Γ_k	0.222
n	–	2
p	–	5

TABLE S2: Parameter values of the dimensionless model

[1] For an excellent introduction to the nonlinear dynamics concepts that will be used in what follows, see Ref. [S7].

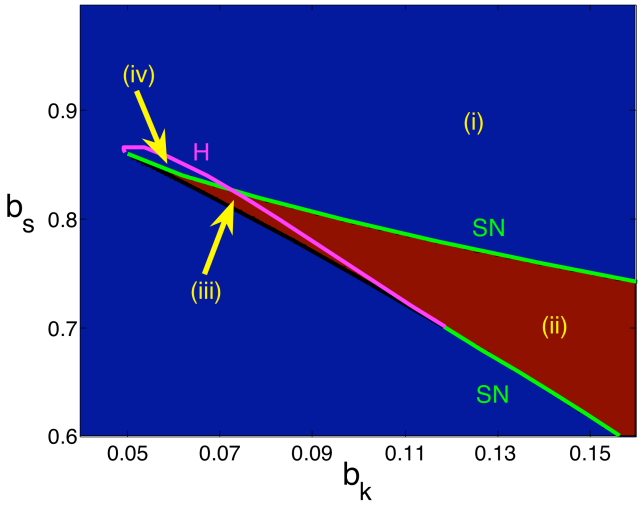

FIG. S2: Phase diagram showing the number of fixed points (in color coding) of model (S10)-(S11) and their instability boundaries. Blue represents a single fixed point and red corresponds to three fixed points. Yellow labels denote different regions described in the text. Parameter values are those of Table S2, except b_k and b_s, which are variable.

The different instability lines described above delineate four different regions, denoted by yellow numbers in Fig. S2, that can be described as follows:

(i) Monostability: only one fixed point exists, and it is stable. Typical phase-plane nullcline portraits are shown in Figs. S3A (vegetative state) and S3B (competent state).

(ii) Bistability: three fixed points exist, two of which are stable. The vegetative and the competent regimes coexist. A typical phase-plane nullcline portrait is shown in Fig. S3C. In that figure, the two stable fixed points are denoted by full circles, and the unstable saddle at intermediate values of ComK is represented by an empty circle.

(iii) Excitability: three fixed points exist, but only one of them is stable. The competent fixed point is an unstable spiral, and the mid-ComK fixed point remains a saddle point. Large enough perturbations will excite the system out of the vegetative state into the competence region, which can be interpreted as the area around the unstable spiral fixed point. A typical phase-plane nullcline portrait is shown in Fig. S3D.

(iv) Limit cycle oscillations: only one fixed point exists, but it is *unstable*. The system exhibits limit cycle oscillations between a mid-ComK and a high-ComK level.

The portion of SN boundary separating regions (iii) and (iv) corresponds to a homoclinic bifurcation. The limit cycle that exists in region (iv) disappears upon entering region (iii), after colliding with the newly born saddle point located at intermediate ComK levels (see Fig. S3C). In that way, within the excitability region no limit cycle exists, the only attractor being the vegetative fixed point.

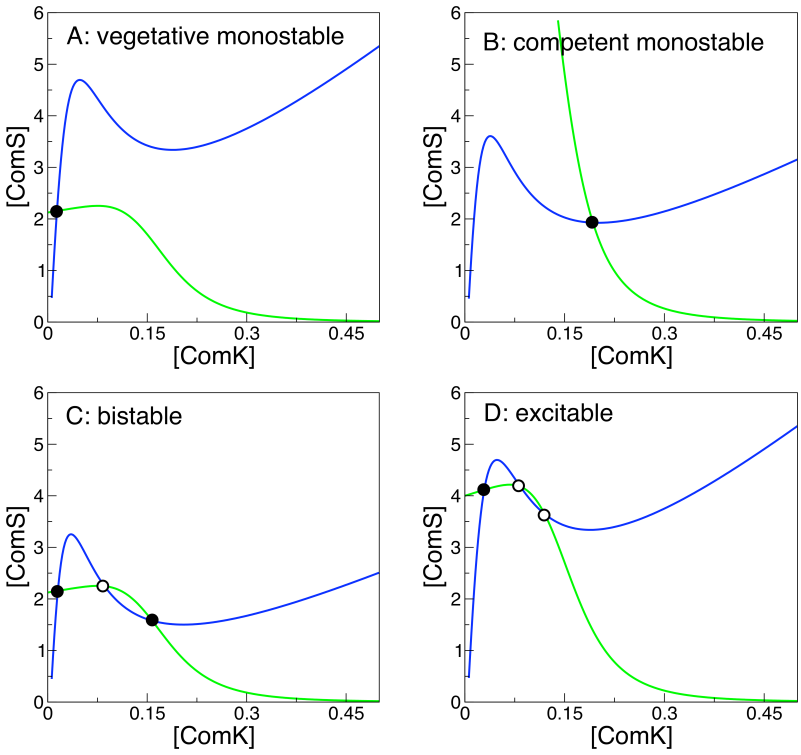

FIG. S3: Typical phase-plane nullcline portraits corresponding to regions (i)-(iii) in Fig. S2. The blue line corresponds to the ComK nullcline, and the green line to the ComS nullcline. Furthermore, the filled black dots denote stable fixed points, and the empty ones correspond to unstable fixed points. Parameter values are those of Table S2, except: (A) $b_k = 0.08$, $b_s = 0.68$, (B) $b_k = 0.12$, $b_s = 0.92$, (C) $b_k = 0.14$, $b_s = 0.68$, and (D) $b_k = 0.08$, $b_s = 0.8$.

S2.C. Exciting competence

Let us now concentrate on the excitable regime existing in region (iii) of the phase diagram shown in Fig. S2 (see also Fig. S3C). As mentioned earlier, a sufficiently large perturbation of the vegetative state will excite a large-amplitude excursion through the competence region in phase space. Stochasticity of gene regulation provides a rich source of such perturbations. We have considered three different possible sources of competence-triggering fluctuations:

1. Multiplicative noise acting parametrically on b_s:

$$\frac{dS}{dt} = \frac{b_s + \xi(t)}{1 + (K/k_1)^p} - \frac{S}{1 + K + S}$$

2. Additive noise acting on ComS promoter activity:

$$\frac{dS}{dt} = \frac{b_s}{1 + (K/k_1)^p} - \frac{S}{1 + K + S} + \xi(t)$$

3. Additive noise acting on ComK promoter activity:

$$\frac{dK}{dt} = a_k + \frac{b_k K^n}{k_0^n + K^n} - \frac{K}{1 + K + S} + \xi(t)$$

In all cases, we use a Gaussian noise with zero mean and an exponentially decaying correlation in time

$$\langle \xi(t)\xi(t')\rangle = \frac{D}{\tau_c}\exp\left(-\frac{|t-t'|}{\tau_c}\right)$$

This is the so-called Ornstein-Uhlenbeck noise. The choice of this type of correlation is motivated by recent studies in gene expression noise dynamics [S2]. The correlation time is taken to be roughly of the order of the cell-cycle duration. Noise with shorter correlation times also trigger competence and may be more compatible with sister cell results. We have checked that all three types of perturbations are able to trigger competence events in the system. Furthermore, we note that in the presence of time-correlated noise, competence events can also be excited outside (below) region (iii), when fluctuations take the cell transiently within that region. The values of the noise parameters used in this paper are $D = 0.01$ and $\tau_c = 3$, which correspond to a noise amplitude $\sqrt{D/\tau_c} = 0.058$ in dimensionless units. This value is approximately 7% of the full expression level of ComS, given by $b_s = 0.82$.

S2.D. Delayed repression of ComS by ComK

The excitable region (iii) shown in the phase diagram of Fig. S2 is rather small. This limitation is removed in the presence of time delay in the repression of ComS expression by ComK. This delay is expected given that this link is indirect. To incorporate the delay, we modify the model substituting Eq. (S11) by

$$\frac{dS}{dt} = \frac{b_s}{1+(K(t-\tau)/k_1)^p} - \frac{S}{1+K+S}\,, \tag{S12}$$

where τ is the delay time, measured in units of $1/\delta_k$.

The time delay has no effect on the stability of either the vegetative fixed point or the saddle at intermediate ComK levels, but does affect the competent fixed point, which is the only spiral point of the dynamics in this area of parameter space. A large enough delay destabilizes this fixed point, as shown schematically in Fig. S4. The result of this destabilization is that the size of region (iii) increases. Delays were previously shown to destabilize stable states in biological systems [S9].

The influence of the delay time on the position of the Hopf instability line is shown in Fig. S5A, as obtained with the continuation software DDE-BIFTOOL [S10]. For small delays the Hopf line moves upwards, so that the size of the region where the competent fixed point is unstable increases. This in turn increases the region of excitability, which is the portion of red area where that fixed point is unstable. For larger delays (e.g. $\tau = 1.08$, corresponding to a delay time of approximately 12 min, and shown by a yellow line in plot S5A) a second Hopf instability line comes from above. Collision between the two lines (see e.g. the green line corresponding to $\tau = 1.1$) increases substantially the region of instability of the competent fixed point, and for larger τ values that fixed point is unstable everywhere in the plotted region. This tendency is similar for smaller values of the Hill coefficient p, although the values of τ needed to destabilize the competent fixed point in that case are slightly larger (see Fig. S5B). These results show that excitability is a generic feature of this model in the presence of delay.

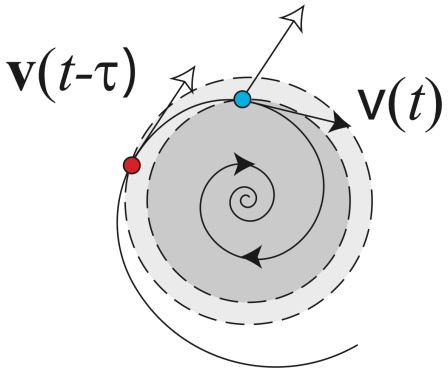

FIG. S4: Qualitative sketch showing the effect of time delay on the stability of a spiral fixed point. At a given time instant, the velocity vector to which the trajectory is tangential is the combination of the previous vector and a delayed one. For large enough delays, this combination begins to point outwards, destabilizing the spiral. Note that this heuristic argument holds close enough to the fixed point, so that a linearization of the dynamics is possible, and for time delays smaller than the characteristic period of the spiral point, even though destabilization occurs even in the absence of this latter requirement.

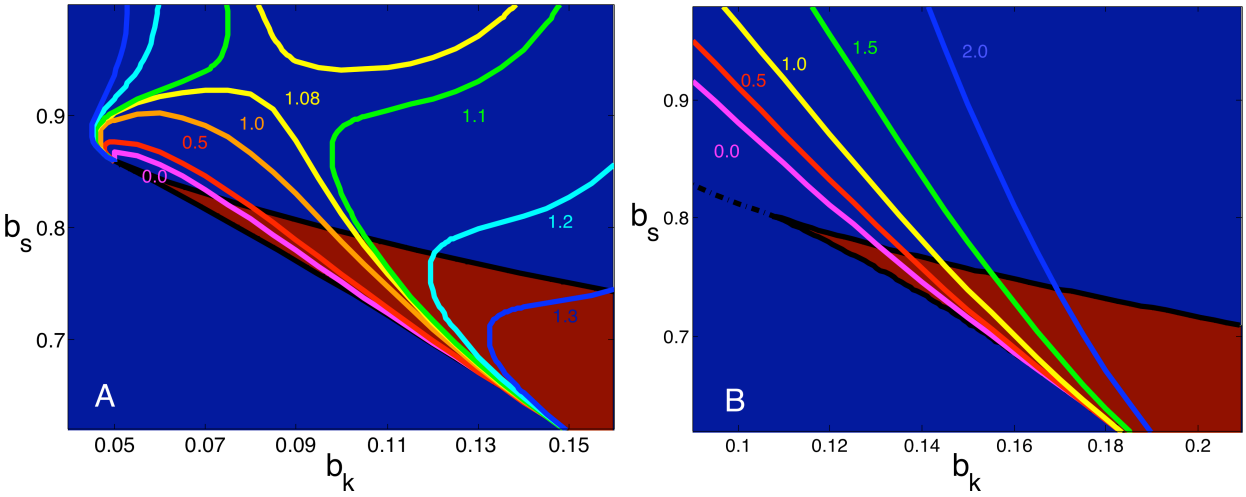

FIG. S5: Effect of increasing time delay on the position of the Hopf instability line (colored lines). The value of the delay time is shown next to each line, in units of $1/\delta_k \approx 12$ min. The solid black lines are the saddle-node bifurcation lines, and the dot-dashed black line in plot B represents a supercritical Hopf boundary which is generic for all values of the delay. Parameter values are those of Table S2, except $p = 2.5$ in plot B.

S2.E. Modeling the effect of feedback bypass

As described in the main text, a Feedback Bypass (FeBy) strain of *B. subtilis* was constructed in which a single chromosomal copy of the pure ComK promoter P_{comG} drives expression of ComS. This is modeled by introducing an extra term into the ComS equation (S11):

$$\frac{dS}{dt} = \frac{b_s}{1+(K/k_1)^p} + \frac{b_g K^n}{k_g^n + K^n} - \frac{S}{1+K+S}\,. \tag{S13}$$

In other words, ComK activates expression of ComS via a Hill function with the same cooperativity coefficient as the positive transcriptional feedback of ComK on itself. We also assume the same concentration value for half-maximal activation, $k_g = k_0 = 0.2$. Figure S6 shows the phase-plane portrait of the system for $b_g = 0.20$. The plot shows that trajectories now tend to the competent fixed point, which has been rendered stable by the feedback bypass link (and whose stability is much larger than that of the vegetative fixed point). This behavior may be compared with Fig. 5 (main text).

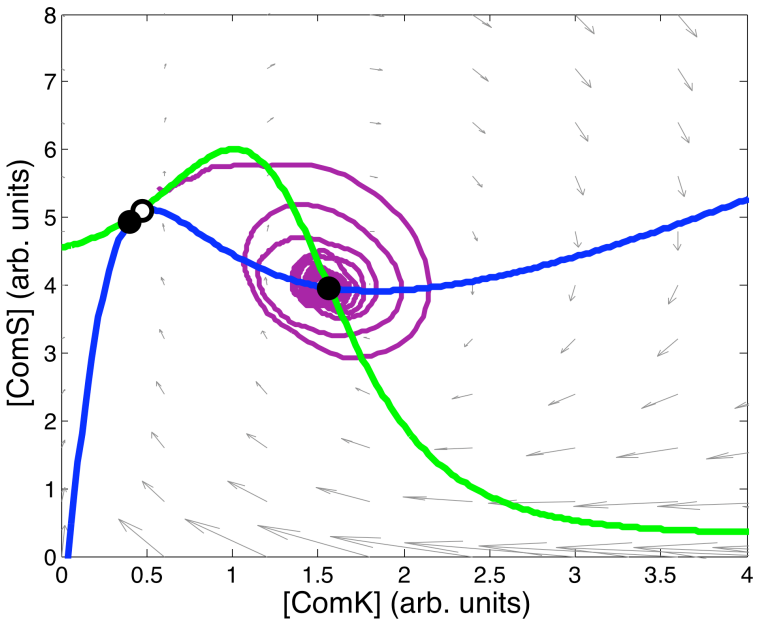

FIG. S6: Phase plane portrait of the feedback bypass system. The competent fixed point is now stable (rightmost full circle).

S3. COMPARING EXCURSION TIMES IN SISTER CELLS

In order to check whether competent sister cells are more likely to exhibit similar excursion times because they share initial conditions, we have statistically analyzed the difference between excursion times in sister cells and in the general cell population. The resulting cumulative histograms are plotted in Fig. S7. As can be seen, the two distributions are highly similar as determined by the Kolmogorov-Smirnov test ($p = 0.89$). Simulations of the MeKS model yield qualitatively similar results, as shown in Fig. S8 (compare with Fig. 3e, main text).

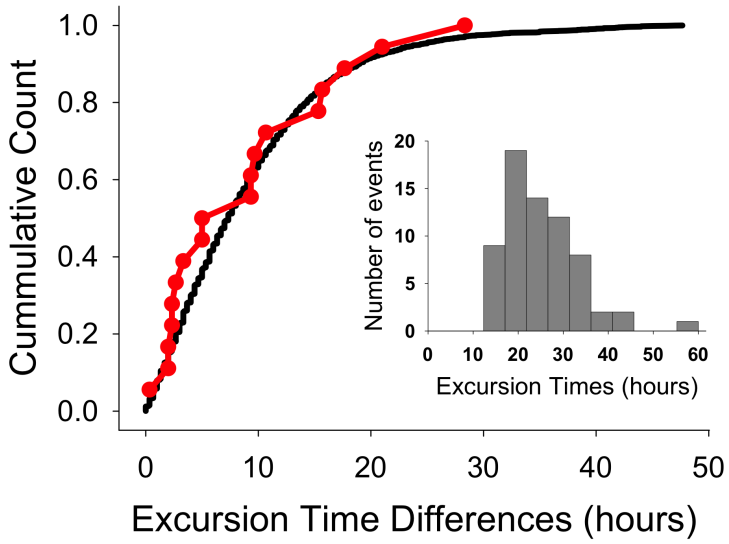

FIG. S7: Cumulative histograms of differences between excursion times as measured experimentally. Shown in black is the cumulative histogram of differences between all competence events recorded. In red, cumulative histogram of differences between sister cell competence events. The inset shows the histogram of excursion times for all the measured events.

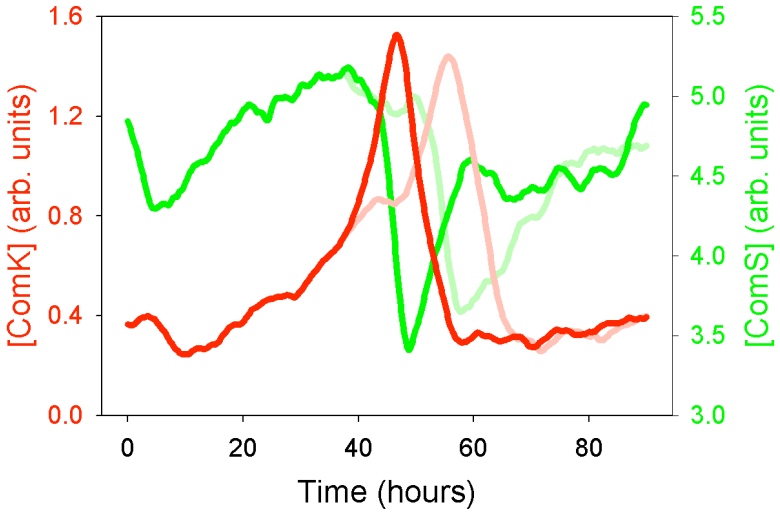

FIG. S8: Numerically simulated time traces of two sister cells undergoing competence. ComK traces are shown in shades of red and ComS in shades of green. Compare with Fig. 3e (main text).

S4. ADDITIONAL SUPPLEMENTARY FIGURES

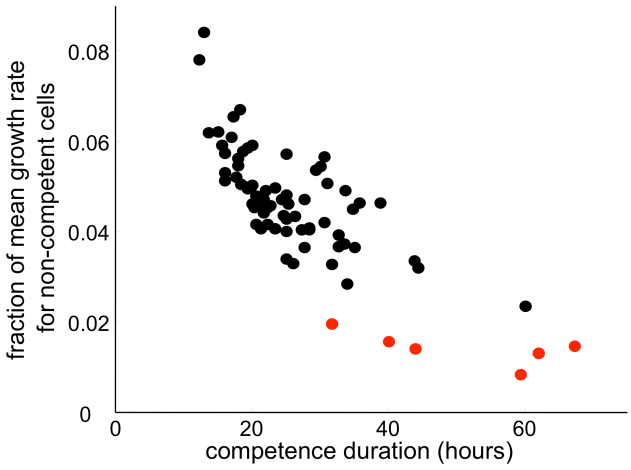

FIG. S9: **Competence retards cellular growth.** Shown in black (red) are single-cell competent events from the wild-type (FeBy) strain. Competence duration of FeBy cells is defined as the time between entry into competence and cell death due to phototoxicity. Growth rate refers to the mean logarithmic increase in total cell length per unit time during competence, normalized by the growth rate of non-competent cells. Note that compared to competent cells, non-competent cells have at least a ten-fold slower growth rate.

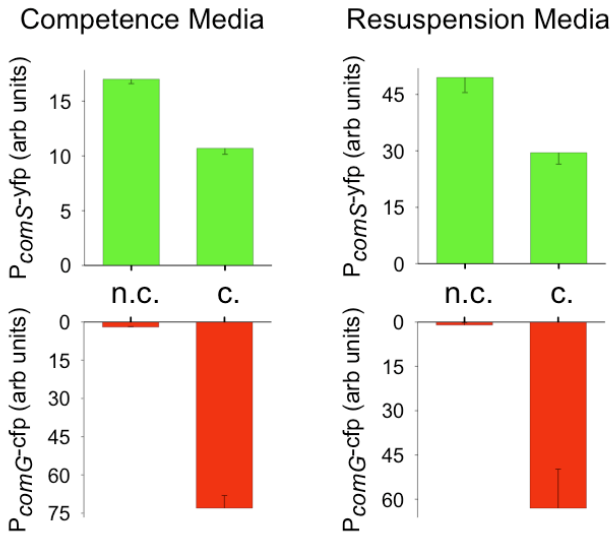

FIG. S10: **Comparing competence and resuspension media.** Shown are mean P$_{comS}$-*yfp* (green color) and P$_{comG}$-*cfp* (red color) expression in non-competent (n.c.) and competent (c) cells in competence and resuspension media. Note that the relative reduction in comS expression is the same (∼60%) in both media, despite a change in the absolute expression level. These data show that the repression of P$_{comS}$-*yfp* in competent cells is qualitatively similar in both RM and CM media.

[S1] Sterlini, J. M. & Mandelstam, J. Commitment to sporulation in *Bacillus subtilis* and its relationship to development of actinomycin resistance. Biochem J **113**, 29–37 (1969).

[S2] Rosenfeld, N., Young, J. W., Alon, U., Swain, P. S. & Elowitz, M. B. Gene regulation at the single-cell level. Science **307**, 1962–5 (2005).

[S3] Dubnau, D., Davidoff-Abelson, R. & Smith, I. Transformation and transduction in *Bacillus subtilis*: evidence for separate modes of recombinant formation. J Mol Biol **45**, 155–79 (1969).

[S4] Grossman, A. D. Genetic networks controlling the initiation of sporulation and the development of genetic competence in *Bacillus subtilis*. Annu Rev Genet **29**, 477-508 (1995).

[S5] Hamoen, L. W., Venema, G. & Kuipers, O. P. Controlling competence in *Bacillus subtilis*: shared use of regulators. Microbiology **149**, 9-17 (2003).

[S6] Lazazzera, B. A. Quorum sensing and starvation: signals for entry into stationary phase. Curr Opin Microbiol **3**, 177–182 (2000).

[S7] Strogatz, S. H., *Nonlinear Dynamics and Chaos* (Addison-Wesley, Reading, 1994).

[S8] http://indy.cs.concordia.ca/auto/

[S9] Lewis, J. Autoinhibition with transcriptional delay: a simple mechanism for the zebrafish somitogenesis oscillator. Curr Biol **13**, 1398-408 (2003).

[S10] Engelborghs, K., Luzyanina, T. & Roose, D. Numerical bifurcation analysis of delay differential equations using DDE-BIFTOOL. ACM Trans Math Softw **28**, 1–21 (2002).